International Symposium
On Turbulence and Shear Flow
Phenomena (TSFP-8)
August 28 - 30, 2013 Poitiers, France

SUBOPTIMAL CONTROL OF WALL TURBULENCE WITH MOVING DIMPLES

W.-X. Huang
Department of Engineering Mechanics
Tsinghua University
Beijing 100084, China
email: hwx@tsinghua.edu.cn

W.-Y. Zhang
Department of Engineering Mechanics
Tsinghua University
Beijing 100084, China

M.-W. Ge
Department of Engineering Mechanics
Tsinghua University
Beijing 100084, China

G. Yang
Department of Engineering Mechanics
Tsinghua University
Beijing 100084, China

C.-X. Xu
Department of Engineering Mechanics
Tsinghua University
Beijing 100084, China
email: xucx@tsinghua.edu.cn

ABSTRACT

Direct numerical simulation of a turbulent channel flow with moving dimples at the bottom wall was carried out using the spectral method. Suboptimal control based on the wall information of the spanwise wall shear stress was applied for skin-friction drag reduction. The average reconstruction scheme together with the spanwise stripped truncation of the weighting function was found to be effective for realization of the control law in physical space. Both the linearized approximate and real no-slip boundary conditions were tested. It was found that the approximate boundary condition overestimates the drag reduction rate. For the real no-slip condition, low-pass filtering of the wall shear stress was additionally implemented for the control input to eliminate the fluctuations due to the presence of dimples. Drag reduction was successfully obtained by reducing the pressure form drag as compared with the original suboptimal control.

INTRODUCTION

Effective control of wall-bounded turbulent flows for skin-friction drag reduction is of significance in scientific research as well as in engineering problems. During the past several decades, there is a rapid progress in understanding the self-sustenance or regeneration mechanism of near-wall turbulence. Hence, various control strategies have been developed, aiming at reducing the skin friction drag, by intervening in the regeneration cycle of near-wall turbulence. For instance, the opposition control scheme proposed by Choi et al. (1994) used the blowing/suction through the wall to counteract the sweep and ejection motions induced by streamwise vortices in buffer layer. Inspired by this intuitive but successful idea, more practical control laws were then found by employing information measurable at the wall, e.g. the neural network (Lee et al. 1997) and the suboptimal control (Lee et al. 1998). On the other hand, instead of the blowing/suction through the wall, the deformable wall was then adopted in the opposition control (Kang and Choi 2000). From the practical point of view, the real wall surface cannot be deformed continuously. Endo et al.

(2000) presented a new design consisting of arrays of sensors and actuators of finite dimensions at the wall. The actuators are deformable and elongated in the streamwise direction, while the sensors capture the wall information as input of actuators. An explicit control scheme was proposed, based on the spanwise gradient of wall shear stress due to its correlation with the near-wall coherent structures, and about 10% drag reduction was obtained for Re_τ=150. Noteworthily, development of MEMS technology in recent years increased the feasibility and potential of such active control strategy in real applications. In the present study, we applied the suboptimal control on the turbulent channel flow for drag reduction by moving circular dimple actuators via direct numerical simulations.

CONTROL STRATEGIES

The computational domain is plotted in Fig. 1(a). We consider a turbulent channel flow with sensors and actuators distributed in an interlaced pattern at the bottom wall, as shown in Fig. 1(b). The sensor is flat and undeformed, while the actuator is able to be deformed into a dimpled shape (Fig. 1(c)). The center velocity of the dimple is determined according to the suboptimal control strategy. A cost functional based on the spanwise wall shear stress was adopted, as proposed by Lee et al. [3], i.e.

$$\mathcal{J}(\phi)=\frac{1}{2A\Delta t}\int_S\int_t^{t+\Delta t}\left[l\phi^2-\left(\partial w/\partial y\right)_{\mathrm{w}}^2\right]\mathrm{d}t\mathrm{d}S \qquad (1)$$

where ϕ denotes the actuation signal, which uses the normal velocity of the dimple center in the present study, A denotes the wall area, Δt denotes the time interval, and l denotes an adjustable constant reflecting the relative price of control. By using the variational method, a simple relationship between the wall normal velocity and the spanwise wall shear stress was obtained in the spectral space, i.e.

$$\hat{\phi}=C\frac{ik_z}{|k_z|}\widehat{\frac{\partial w}{\partial y}}\bigg|_w \qquad (2)$$

where the symbol with caret denotes the corresponding Fourier coefficient, and C denotes a positive scale factor. In the present study, the control law (Eq. (2)) was transformed into the physical space, i.e.

$$\phi\left(x_j,z_k\right)=C\sum_{j'}\sum_{k'}W^{\mathrm{w}}_{j'k'}\frac{\partial w}{\partial y}\bigg|_{\mathrm{w}}\left(x_{j+j'},z_{k+k'}\right) \qquad (3)$$

where W denotes the weighting function, which is the Fourier transform of the coefficient $ik_z/|k_z|$, as plotted in Fig. 2. It is seen that the weighting function is symmetric in the streamwise direction but is asymmetric in the spanwise direction. Although the exact form of the weighting function extends into the whole wall, it decays fast as the distance increases. Thus, a truncation of the weighting function was made for practical purposes. Moreover, the information of wall shear stress outside the sensor area has to be reconstructed based on that obtained from the sensors.

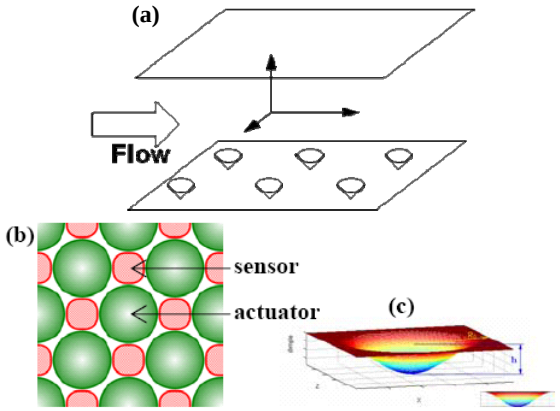

Figure 1. (a) Computational domain; (b) Arrangement of sensors and actuators; (c) Dimple profile

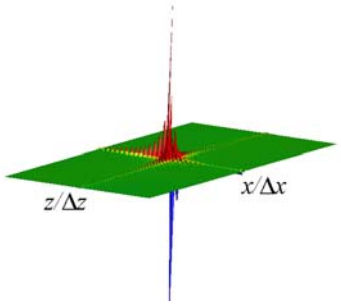

Figure 2. Distribution of the weighting function

The incompressible Navier-Stokes equations written in the rotational form and the continuity equation were used as the governing equations, i.e.

$$\frac{\partial\vec{V}}{\partial t}=\vec{F}-\nabla\Pi+\frac{1}{\mathrm{Re}}\nabla^2\vec{V} \qquad (4)$$

$$\nabla\cdot\vec{V}=0 \qquad (5)$$

where $\vec{V}$ denotes the velocity vector, $\vec{F}=\vec{V}\times\vec{\omega}$, $\vec{\omega}=\nabla\times\vec{V}$, and $\Pi=p/\rho+\left|\vec{V}\right|^2/2$ denotes the total pressure. Eqs. (4) and (5) were solved by the pseudo-spectral method in conjunction with a third-order time-splitting scheme (Xu et al. 1996). The periodic condition was used in the streamwise and spanwise directions with constant mass flux, and the no-slip boundary condition was applied at the top wall. For the bottom wall, two strategies were considered to handle the wall deformation. One is to satisfy the accurate no-slip condition by adopting the curvilinear coordinate system. In computation, a coordinate transformation is introduced to map the irregular physical domain into a rectangular computational domain (Ge et al.

2010). The other is to use the linearized approximate boundary condition by assuming the small displacement of the bottom wall, i.e.

$$u_i^{LB} = \frac{\partial f}{\partial t}\delta_{i2} - f\left(x,z,t\right)\frac{\partial u_i^{LB}}{\partial y}, \qquad (6)$$

where f denotes the wall displacement from its equilibrium position. Using Eq. (6), the governing equations were solved on the original rectangular grids and the computational cost was significantly reduced as compared with the accurate method. To test the validity of the approximate method, we simulated a laminar channel flow with a single oscillating dimple at the bottom wall. Figure 3 shows the streamwise and normal velocity profiles at the instant when the dimple reaches its maximum velocity, obtained by both the accurate and approximate methods. Although some deviations are observed, we assert that the approximate method does not cause qualitative difference with the accurate method, since the control strength can also be adjusted by the scale parameter in Eq. (3).

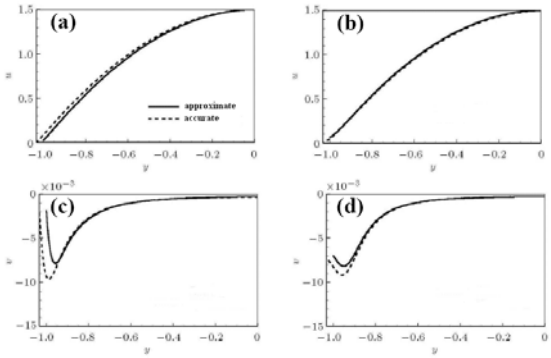

Figure 3. Streamwise (a,b) and normal (c,d) velocity profiles at the front edge (a,c) and middle (b,d) of the dimple

NUMERICAL RESULTS

In the present simulations, the Reynolds number based on the mean bulk velocity and the channel half-height is 2850. The domain size is $2\pi \times 2 \times \pi$ in the streamwise, normal and spanwise directions respectively, and the corresponding grid numbers are $128 \times 65 \times 128$. At the bottom wall, total $32 \times 32 \times 2$ sensors and dimple actuators are arranged, and the diameter of the dimple is about 10 viscous wall units. The scale parameter in Eq. (1) is set to be C=1×10^{-3}.

Table 1: Skin-friction drag of turbulent channel flow

Control scheme	Average friction	Drag reduction rate (%)
No control	12.90	0
Opposition dimple control	11.97	7.21
Suboptimal dimple control cross 11×3∪3×11 average rebuilding	11.22	13.02
Suboptimal dimple control cross 11×3∪3×11 interpolation rebuilding	11.31	12.32
Suboptimal dimple control spanwise rectangle 3×11 average rebuilding	11.24	12.87

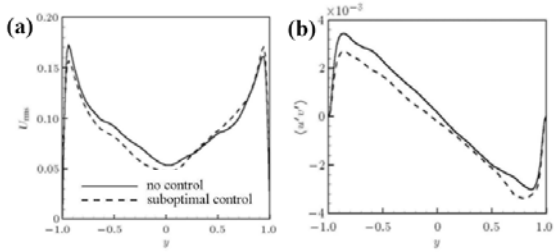

Figure 4. Profiles of the root mean square of the streamwise velocity fluctuation (a) and Reynolds stress (b)

Approximate method

Using the approximate method, the reconstruction of wall shear stress and the truncation of the weighting function were first tested. As seen in table 1, the average scheme and the linear interpolation scheme for reconstruction were found to yield similar drag reduction rates, about 13%, since the dimple size was set to be comparable to that of the cross section of the near-wall streamwise vortices. Moreover, the cross truncation containing four sensors produces only a slightly larger drag reduction rate than that of the spanwise stripped truncation containing two sensors, indicating that the distribution of wall shear stress along the spanwise direction is essential for suboptimal control rather than the streamwise direction. Interestingly, the results of opposition control with moving dimples are also included in table 1, which is found to less effective than the suboptimal control due to the limitation imposed by the actuator size, unlike that with continuous moving wall (Kang & Choi 2000) or blowing/suction (Choi et al. 1994). In the following, the spanwise stripped truncation together with the average reconstruction was adopted, by considering both the control effectiveness and the computational cost. Figure 4 shows the profiles of the root mean square of the streamwise velocity fluctuation and

the Reynolds stress, both of which are decreased obviously as compared with the no control case.

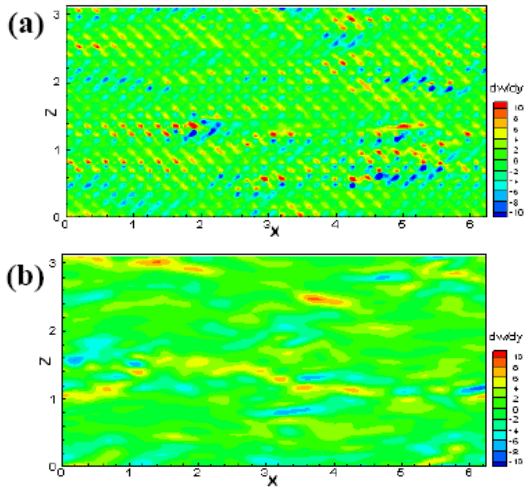

Figure 5. Contours of the spanwise wall shear stress on (a) the dimpled wall and (b) the flat wall.

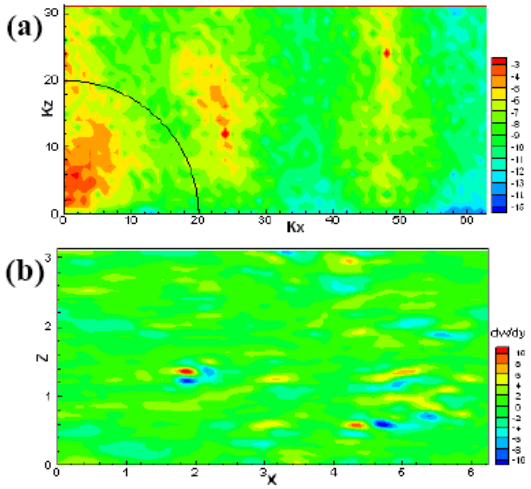

Figure 6. Distributions of (a) the original spanwise wall shear stress on the dimpled wall in the spectral space and (b) the spanwise wall shear stress after low-pass filtering in the physical space. The solid line in (a) denotes the boundary of wavenumber for low-pass filtering.

Accurate method

For the real no-slip boundary condition, the simulations were carried out using the moving curvilinear coordinate system. First the spanwise wall shear stress was examined, since it is used as the input signal for the suboptimal control. Figure 5 shows a comparison of the distribution of the spanwise wall shear stress on the dimpled wall with that of the no-controlled flat wall. It is seen that that the spanwise wall shear stress is contaminated due to the presence of dimples, and thus the wall information cannot effectively reflect the influence of near-wall coherent structures. To solve this problem, we used a low-pass filter to eliminate the high-frequency fluctuations of the spanwise wall shear stress. Figure 6(a) presents the distributions of the original spanwise wall shear stress on the dimpled wall in the spectral space. We can see that high energy concentrations are present at high wavenumbers in both the streamwise and spanwise directions, which correspond to the spacing of dimples on the bottom wall. A low-pass filtering was implemented in the present study by using the spectrum truncation, with the boundary of truncation wavenumber plotted in the Fig. 6(a). After the low-pass filtering, the spanwise wall shear stress is shown in Fig. 6(b), which resembles the flat wall case as seen in Fig. 6(b), indicating that the contamination of the spanwise wall shear stress due to the dimples was effectively eliminated. The filtered stress was then used as the input signal for suboptimal control.

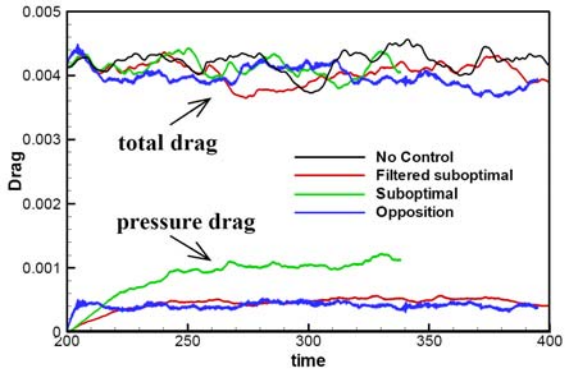

Figure 7. Time histories of the skin friction drag

Time histories of total drag and pressure drag of the bottom wall are displayed in Fig. 7, where the suboptimal, opposition and no control cases are included for comparison. We can see that there is about 3% reduction in the total drag for the filtered suboptimal control, similar with the opposition control case, while no drag reduction is obtained for the original suboptimal control, due to the increase of the pressure drag. Figure 8 displays the instantaneous position of the dimples and the corresponding normal velocity on the bottom wall. For the original suboptimal control (Fig. 8(a)), it is observed that the dimples become static gradually due to the contamination of the input signal, and the pressure form drag is thus increased significantly. On the other hand, by adopting the filtered suboptimal control scheme (Fig. 8(b)), the dimples form a streamwise elongated pattern, reflecting the effect of the near-wall low speed streaks. As a result,

the pressure form drag is reduced as compared with the original suboptimal control. For comparison, the instantaneous dimple motion using the opposition control is displayed in Fig. 8(c). We can also see an elongated pattern of dimples in the streamwise direction, similar with the filtered suboptimal control, while the variation of the normal velocity of dimples is more violent for the opposition control.

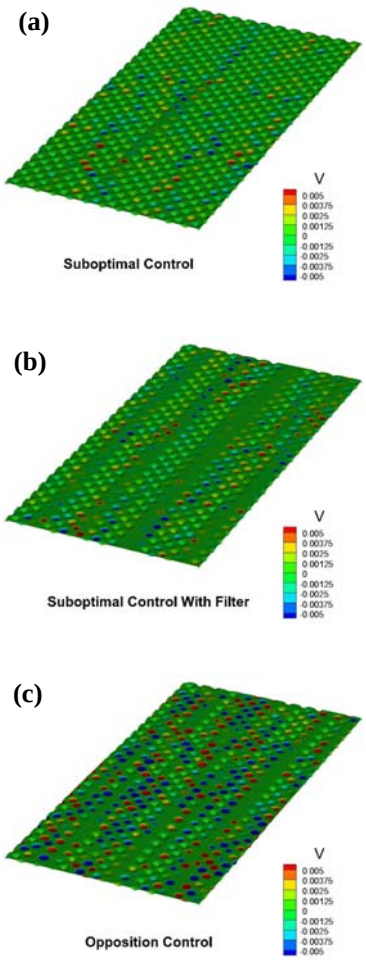

Figure 8. Instantaneous position of dimples and the corresponding normal velocity on the bottom wall by different control schemes: (a) original suboptimal control; (b) filtered suboptimal control; (c) opposition control.

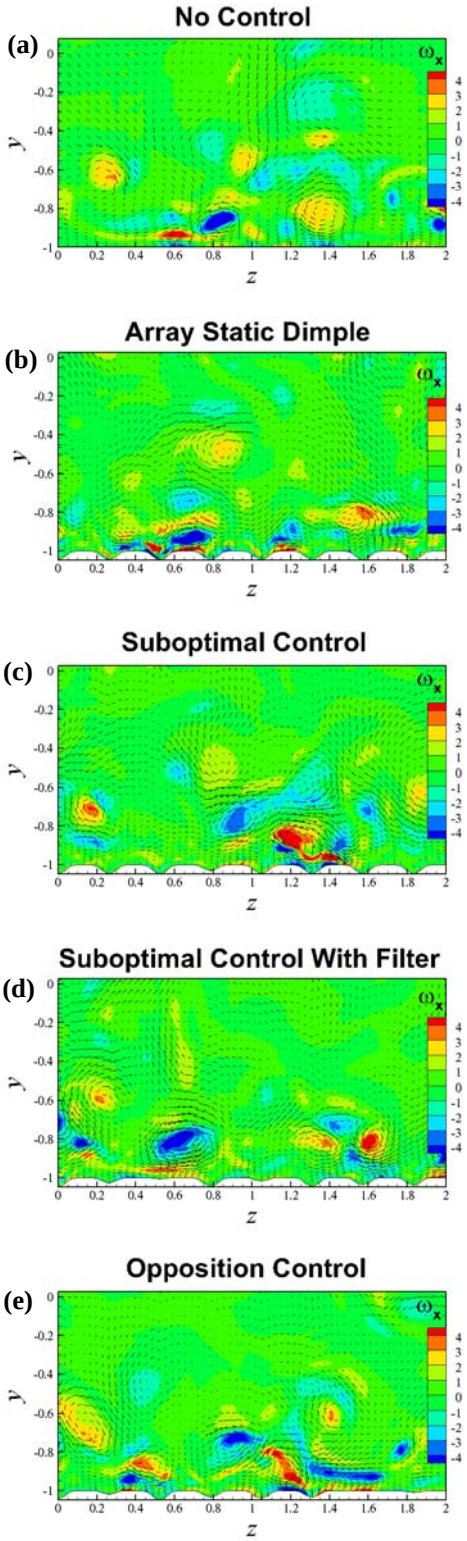

Figure 9. Instantaneous velocity vector field together with the streamwise vorticity at the cross section: (a) no control flat wall case; (b) static dimpled wall case; (c) original suboptimal control; (d) filtered suboptimal control; (e) opposition control.

Then we examined the instantaneous velocity field together with the streamwise vorticity in the cross section perpendicular to the streamwise direction, as shown in Fig. 9, where we included the three control schemes, i.e. the opposition control, the original suboptimal control and the filtered suboptimal control, the no control flat wall case, and the static dimpled wall case. For the no control flat wall case (Fig. 9a), there are alternating signed streamwise vortices along the spanwise direction, which induce reversed flow on the bottom wall. For the static dimpled wall case (Fig. 9b), it is shown that the down washing flow induced by the streamwise vortices collides the dimple edges, resulting in more complex flow patterns on the dimpled wall. For the original suboptimal control (Fig. 9c), the dimples gradually become static as shown above (Fig. 8a), and thus collision of the down washing flow on the dimple edges is also observed. Furthermore, for the filtered suboptimal control (Fig. 9d), the dimples are continuously deforming according to the input signal, and such collision is found to be attenuated. On the other hand, for the opposition control (Fig. 9e), since the dimple shape varies violently as shown above (Fig. 8c), the collision of the down washing flow on the dimple edges is still observed and the attenuation of the near wall streamwise structure is not obviously shown.

CONCLUSIONS

The suboptimal control was applied in the turbulent channel flow using moving dimples at the bottom wall for skin-friction drag reduction. The dimple size was set to be comparable to that of the cross section of the near-wall streamwise vortices. The wall shear stress outside the sensor area was reconstructed from the sensor information for realization of the control law in physical space. The average reconstruction scheme together with the spanwise stripped truncation of the weighting function was found to be effective. Using the linearized approximate boundary condition, about 13% drag reduction rate was achieved, higher than that of the opposition control with moving dimples. However, using the real no-slip condition, low-pass filtering of the wall shear stress has to be applied to eliminate the fluctuations due to the presence of dimples. Finally, about 3% drag reduction rate was obtained under the real no-slip condition, indicating that the approximate boundary condition overestimates the drag reduction rate.

ACKNOWLEDGMENTS

The work was supported by National Natural Science Foundation of China (Grant No. 11002081, 10925210 and 11132005).

REFERENCES

Choi, H., Moin, P., Kim, J., 1994, “Active turbulence control for drag reduction in wall-bounded flows”, *J. Fluid Mech.*, vol. 262, pp. 75.

Endo, T, Kasagi, N., Suzuki, Y., 2000, “Feedback control of wall turbulence with wall deformation”, *Int. J. Heat Fluid Flow,* vol. 21, pp. 568.

Ge, M.W., Xu, C.X. & Cui G.X., 2010, “Direct numerical simulation of flow in channel with time-dependent wall geometry”, *Appl. Math. Mech.*, vol. 31, pp. 97.

Kang, S., Choi, H., 2000, “Active wall motions for skin-friction drag reduction”, *Phys. Fluids,* vol. 12, pp. 3301.

Lee, C., Kim, J., Babcock, D., Goodman, R., 1997, “Application of neural networks to turbulence control for drag reduction”, *Phys. Fluids,* vol. 9, pp. 1740.

Lee, C., Kim, J., Choi, H., 1998, “Suboptimal control of turbulent channel flow for drag reduction”, *J. Fluid Mech.*, vol. 358, pp. 245.

Xu, C., Zhang, Z., den Toonder, J.M.J., Nieuwstadt, F.T.M., 1996, “Origin of high kurtosis levels in the viscous sublayer. Direct numerical simulation and experiment”, *Phys. Fluids*, vol. 8, pp. 1938.